Universidad Zaragoza
1542

ECN

Master thesis

Trabajo Fin de Master

Development of a model for computing tip loss corrections in wind turbines

Author:

Andrea Matiz Chicacausa

Supervisors:

PhD. Gerard Schepers

PhD. Cristobal Cortes

Master oficial en Energías Renovables y Eficiencia Energética

June 12, 2013

Resumen

A la fecha, la comprensión de la relación entre el comportamiento de la curva de potencia en una turbina eólica y su número de álabes parece ser insatisfactoria. Esto se debe en parte a que la teoría Blade Element Momentum (BEM), que es la herramienta más usada para modelar el comportamiento aerodinámico de las turbinas, asume un rotor con infinito número de álabes [1, 2, 3, 4]. Esta suposición simplifica el análisis en la medida en que el rotor, a diferencia de las turbinas eólicas reales, es descrito como un disco continuo que gira con una velocidad de rotación determinada. A su vez, hay diferentes fénomenos físicos que suceden en el álabe y que no pueden ser captados por esta teoría. Por ejemplo, la pérdida de potencia en la punta se explica en parte por la no-uniformidad de flujo causada por la presencia de un número finito de álabes en el rotor.

Algunas correcciones realizadas para modelar la pérdida de potencia en las puntas tratan de incluir como parámetros importantes un número finito de álabes y la relación de velocidad en la punta λ. Los resultados de estas correcciones no son del todo satisfactorios y generan incertidumbres a la hora de calcular la distribución de cargas sobre el álabe. Es razonable suponer que también hay una relación entre la geometría del álabe y la pérdida de potencia en la punta del mismo; para incluir dicho efecto creemos que el párametro que es necesario considerar es la estructura de la cuerda del álabe en la punta.

La primera corrección para incorporar un número finito de alabes fue presentada de forma analítica por Prandtl hacia la década de 1920. Él mostró que la pérdida de potencia decae de manera exponencial en la cercanía de la punta del álabe. Esta corrección tiene en cuenta no sólo un número finito de álabes en el rotor sino también la posición radial en el alabe, y corrige la predicción de las fuerzas aerodinamicas calculadas con BEM. En 2005, Wen Z. Shen y sus colegas desarrollaron una corrección que mejora los resultados obtenidos por el modelo de Prandtl [6]. Su propuesta, basada en el análisis empírico de los datos de un proyecto, consiste en agregar un factor de corrección al modelo desarrollado por Prandtl, de manera

que aparece el efecto de la velocidad de rotación sobre las cargas en la punta. Dicho factor correctivo como función de la distancia r del eje del rotor es el siguiente:

$$F(g) = \frac{2}{\pi} \cos^{-1} \exp \left[- g \frac{B(R-r)}{2R \sin \phi_R} \right], \tag{1}$$

donde ϕ_R es el ángulo de flujo, B y R el número y longitud de los álabes. Aquí g es la función exponencial introducida por Shen que depende de λ y que fue hallada empíricamente (si $g = 1$ se obtiene el factor de corrección de Prandtl). A pesar de mejorar notablemente la precisión en el cálculo de las cargas, el modelo de Shen presenta algunas diferencias respecto a los casos de bajas λ.

Con el objetivo de mejorar los resultados obtenidos por Prandtl y Shen este trabajo presenta un nuevo factor de corrección que incluye parámetros que no han sido incluidos en los modelos existentes; por ejemplo, como ya se ha mencionado, la cuerda del álabe. Como resultado, la estructura correctiva de nuestro modelo es la siguiente:

$$F_{\text{new}}(g, s, \sigma) = F(g)\, m(s, \sigma), \quad \text{donde} \quad m(s, \sigma) = 1 - s^{c_3} \exp(-c_4 \sigma) \tag{2}$$

y donde $s = r/R$, σ es el *solidity*[1] y c_3 y c_4 son constantes a-dimensionales estimadas empíricamente. Finalmente, vale le pena añadir que, más allá de estudiar y corregir los modelos de Prandtl y Shen, este trabajo pretende ser un aporte a la mejor comprensión de los fenómenos que ocurren en las puntas de los álabes eólicos.

[1]Esta variable se relaciona con la longitud de la cuerda c mediante la siguiente relación: $\sigma = \frac{Bc}{2\pi r}$.

Contents

Introduction

True be told, the understanding of the power behavior over the blade span (specially at the tip region) in a wind turbine seems to be unsatisfactory. One of the reasons to explain it is that the Blade Element Momentum (BEM) theory, which is the most common tool for computing aerodynamics loads and modeling the behavior of wind turbines, assumes a rotor with an infinite number of blades [1, 2]. The study of wind turbines as continuous discs at high rotational speeds simplifies the aerodynamical analysis and provides good results. However, the fact that real wind turbines have finite number of blades makes that some fluid particles pass through the rotor without any interaction with the blades, producing a non-uniformity on the flow leading into a variation of the induction factor around the rotor, then a loss of lift and hence a loss of power.

In order to compute this power losses it is needed to know the azimuthal variation of the induction factor, but BEM is a limited method for this requirement. For this reason and to correct the assumption of infinite number of blades Prandtl in the decade of 1920 developed a correction factor. This Prandtl's factor takes into account the number of blades and the relation between the local radius and the overall radius of the rotor [3, 4]; and at the same time expresses the ratio between the average induced factor on the rotor plane and the induced velocity at the blade position. Besides, he showed that the power loss goes according to an exponential decay in the vicinity of the tip [5]. Nevertheless, the results obtained with Prandtl correction over predict the aerodynamic loads over the tip of the blade. Therefore, we can think that there are other factors which, at least in principle, could be included in this model; for instance, the chord and the pitch angle of the blade. To date, various tip loss correction models based on original ideas proposed by Prandtl have been developed [6, 7, 8, 9].

In 2005, Wen Z. Shen and coworkers showed the inaccuracy of the existing tip loss correction models when they predict the behavior of the aerodynamical forces (normal force) in the proximity of the tip [6]. Their proposal was based in introducing a new model in order not only to correct the mentioned disagreement but also to include in the model the tip speed ratio and enhance the effect of the number of blades. It is worth to note that while Prandtl's correction is applied to the induced velocities which affect the loads indirectly. Shen's model is applied directly to the loads.

Albeit the correction introduced by means of this model displays a good behavior, there exists some disagreement under low tip speed ratios condition. We believe there is also a relation between the tip loss and the geometry of the blade. since, the relation between the blade and the rotor surface is given by

$$\frac{Bc}{2\pi r}$$

where B is the number of blades, c is the chord of the blade and r the local radius. This parameter is called in the literature the *solidity*.

Motivated by the goal of obtaining a better understanding of the tip loss phenomena, we developed an empirical model, which is presented in this thesis and aims to improve Shen's model. We address the issue of understanding the role played in the tip loss phenomenon by the solidity σ.

Statement of results

Having discussed the motivations of the present work, we will summarize the main results obtained during the development of this master thesis. Before all, it is worth emphasizing that the present model is an empirical one based in experimental observation. We found that a good performance is obtained when we include a function of an exponential type multiplying Shen's model. Therefore, our results suggest that a *new* function $m(s, \sigma)$ depending on the solidity must be included in the following way:

$$F_{\text{new}}(g, s, \sigma) = F(g)\, m(s, \sigma), \qquad \text{where} \qquad F(g) = \frac{2}{\pi} \cos^{-1} \exp\left[- g \frac{B(R-r)}{2R \sin \phi_R} \right]$$

and where ϕ_R is the flow angle at the tip and R is the overall radius of the blade. Here g is the function introduced by Shen, which depends on the number of blades

and the tip speed ratio. The model developed in this work results in a new function which looks like an exponential decay of the following type showed in the next figure.

$$m(s, \sigma) = 1 - s^{c_3} \exp(-c_4 \sigma),$$

where $s = r/R$ is the blade span, c_3 and c_4 are dimensionless constants found empirically from data and equal to 8 and 34.2 respectively.

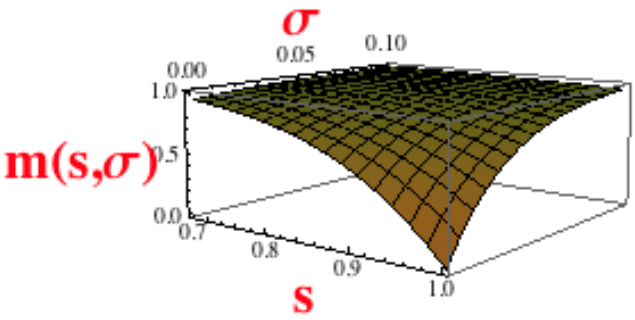

Correcting factor $m(s, \sigma)$. Notice that it is almost everywhere equal to 1 except when s is close to 1 and the chord takes small values.

We summarize the plan of this document by means of the following map shown in next figure. Our framework is the BEM theory, as said. We address the problem of the tip loss as a consequence of the finite number of blades and then we study different proposals for modeling it. In order to develop a new model we have to process the data obtained from the different projects, this means to compute angle of attack when is needed, then filter, clean and averaging data. Finally, we tested the new model with experimental data.

Before finishing this introductory chapter, we give the customary description of the contents of the present work.

- In chapter 1 we review the basic facts about tip loss effect. The main purpose of this chapter is to explain the tip loss phenomena. Finally, at the end of this chapter we provide a brief survey of the tip loss correction models to date.

- Chapter 2 is devoted to the description of the data and the different experimental projects used in the empirical model development. We also offer a preliminary sight of the normal force behavior over the blade for some of the turbines used in this work. The goal of this chapter is to show the characteristics of the turbines over which the new model is based on.

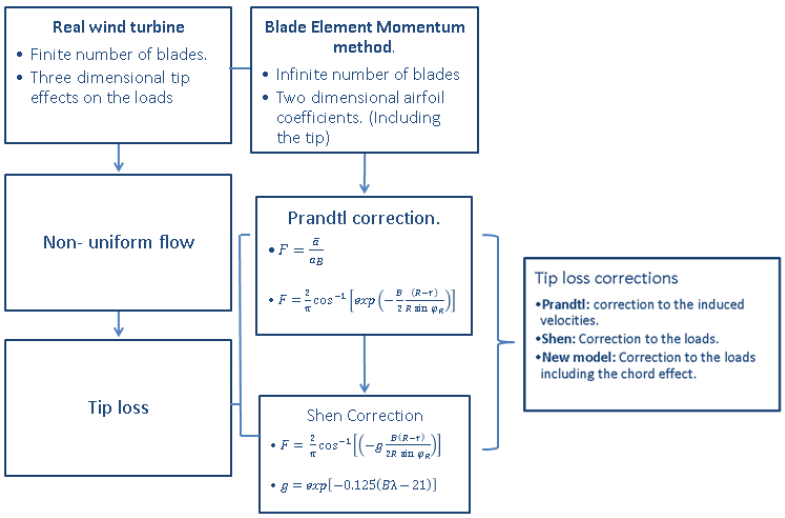

Tip loss diagram.

- In chapter 3 we present the computations done to process the data in order to develop the new model, and finally we show the new model.

- In the last chapter we test the accuracy of the model and offer some conclusions and recommendations for future work.

- We finish this document with three appendices. The first one with a theoretical survey of the aerodynamics basis. The other two present two dimensional data for the airfoils used NREL S809 and NACA n-series.

Ackowledgements

To finalize this chapter I would like to express my deepest gratitude to ECN for supporting my stage here in The Netherlands. Several people made of this time an exciting and enriching experience. Starting with Dr. Gerard Schepers who carried out with the uneasy task of supervise my work and dedicate much of his time to discuss, teach and correct my project. In addition, I would like to thank to all my the colleagues at Wind Energy technologies unit, specially, Dr. Koen Boorsma and Dr. Francesco Grasso, their time and comments made possible succeed in important parts of this work. Besides the support that I had from ECN, Universidad de Zaragoza was also an important part in the development of this project. Dr. Cristobal Cortes who dedicate time to read and correct my work and

in the same way Dr. Inmaculada Arauzo for her good advice when was the time of choosing a supervisor there. Finally, all my best wishes and love for all of those ECN/NRG interns for the nice time we shared, they made this experience much more interesting, multicultural and enriching.

Chapter 1

Tip loss effect

The so-called *tip loss effect* is the power reduction over the outermost part of the blade due mainly to one reason: the effect of the finite number of blades yielding into a non-uniform flow through the rotor. As a result of this non-uniformity, the axial induction factor increases and at the same time the angle of attack and the aerodynamics loads decrease, affecting in this way the lift force.

From one dimensional momentum theory —see Appendix A— the axial induction factor a is defined as the fractional decrease in wind velocity between the free stream and the rotor plane [2]. Then, the velocity at the rotor is the combination of the free stream velocity and the induced velocity, where the axial induction factor increases from zero (far from the rotor). When the rotational effects are introduced there is a loss of energy due to the generation of rotational kinetic energy in the wake behind the rotor, this rotation produces another component to the induced velocity. Then, the induced wind velocity is expressed by means of the angular induction factor a'. Thus, the induced velocity consist of two components: (a) the axial Ua and (b) the orthogonal component in the rotor plane $r\omega a'$.

The *Blade element momentum theory (BEM)* method is based on the assumption of a rotor with an infinite number of blades; in other words, the rotor is represented as an actuator disc [1] —see also Appendix A. Looking at the figure 1.1 it is clear that the inflow angle ϕ is given by the formal expressions:

$$\sin\phi = \frac{(1-a)\,U_\infty}{W} \quad \text{and} \quad \cos\phi = \frac{(1-a)\,\Omega r}{W}, \tag{1.1}$$

where a is the axial induction factor and U_∞ is the wind free stream velocity, W is the relative or effective velocity, Ω is the rotation speed and r is the rotor radius. As soon as ϕ decreases, the lift force will tend to be normal to the rotor plane; and

at the same time, the tangential component of the lift force will tend to be smaller; therefore, the torque will decrease. In this situation, less torque means less power, since $dP = \Omega\, dQ$, where Q is torque and P is power.

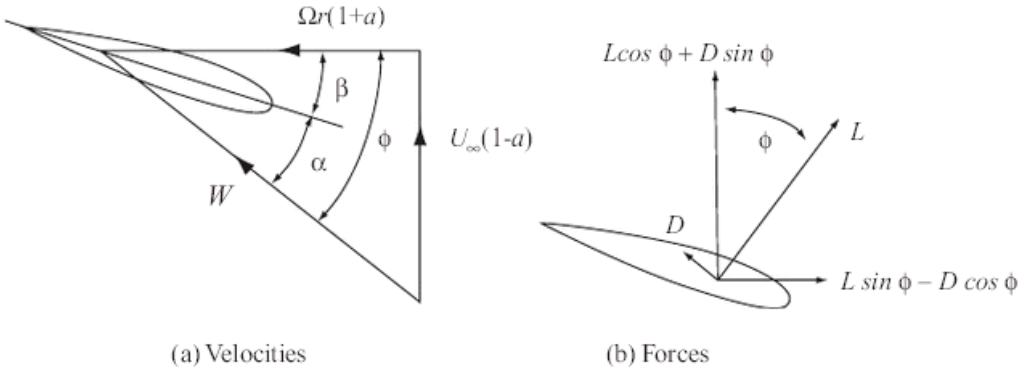

Figure 1.1: Blade element velocities and forces [4].

1.1. Effect of a finite number of blades

Since there is a pressure difference between the sides of the blades the air stream tends to flow around the tip from the lower pressure to the upper pressure surface yielding into the force tend to zero at the tip and hence a reduction of the lift force and the power production. The most straightforward approach for including the tip loss effect in the loads computation and for approximating the assumption of an infinite number of blades to a real rotor is Prandtl's tip loss correction. The so-called Prandtl's factor F has to be introduced into BEM equations —see Appendix A specifically into the axial and angular momentum equations in order to correct the induction factors a and a'. respectively.

Now, once can think that close to the rotor center, the wind turbine behaves closer to a continuos disc; on the other hand, approaching to the blade tip we are far away from a continuos disc behavior, that is because the surface of the blade is given by $\frac{Bc}{2\pi r}$, where B is the number of blades, c is the chord of the blade and r the blade span. Then, the probability of an air particle passing through the rotor without interact with any blade is given by

$$1 - \frac{Bc}{2\pi r}.$$

When r is small it is possible to think that mostly all particles will interact with the blades, but as far as they are from the root the effects due to a finite number of blades increase. It is now clear that the effects of considering a discrete number of blades are more dramatic close to the tip.

1.1.1. Non-uniformity of the flow through the rotor

To obtain the maximum power, the vortex circulation along the blade must be uniform. This will be reach, according to Betz, in an ideal turbine when $a = 1/3$ [1, 3, 4] —see Appendix A. However, this circulation condition is not accomplish in a real wind turbine where the flow behind the rotor rotates in the opposite direction and the tip vortex causes high values of a; then, a will change over the blade and as Prandtl states the circulation at the tip will tend to zero exponentially. This change makes the flow non-uniform leading to the presence of tip loss effect.

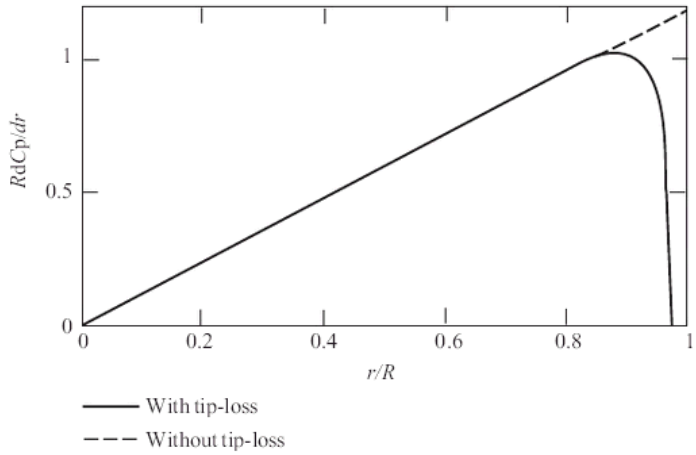

Figure 1.2: Power variation over the blade with and without tip loss [4].

The comparison between a blade with and without tip loss is shown in figure 1.2, where is plotted the power coefficient over the blade span. The behavior of this coefficient leads us to conclude that the tip loss effect only occurs at the outermost part of the blade (approximately higher than 90% blade span). To better understand the effect of the non-uniformity of the flow over the blade it is worth following the path of the air particles approaching to the rotor disc [4]. In fact, as a consequence of their non-homogeneous behavior the particles crossing the rotor can be divided in four sets:

- Particles passing close to and in front of a blade. These particles will leave the trailing edge accelerated in the tangential direction.
- Particles which pass close to the downwind, low pressure surface. These are accelerated tangentially in the opposite direction to the blade motion and then slow down, leaving the trailing edge with the same axial and tangential velocity components as the first particle but on the downwind side of the vortex sheet, additionally they will have a radially inwards velocity.
- A third set of particles which pass between two blades. These particles will be moved axially at a higher velocity than the first two sets of particles, and will be directed into a helical path. They will be faster axially than the vortex sheet ahead the particles will begin to catch up and do not lose as much axial momentum as the first two sets of particles.
- Finally, a fourth set of particles pass between two blades but to a radial position closer to the axis of rotation. The axial velocity of these particles is equal to that of the vortex sheets. If these particles passes midway between two blades, then they will remain midway between the two corresponding vortex sheets. These particles are not affected by the fact that there is a discretized number of blades and follows the same progress as if it were passing through a uniform actuator disc.

This non-uniformity explains why there is a pressure difference between the sides of the blade, which results in that the air tends to circulate around the tip from the lower region to the upper.

1.2. Tip loss correction models

1.2.1. Prandtl tip loss factor

Prandtl developed his correction assuming that the helical sheets in the wake can be replaced by a successions of vortex discs moving with a constant speed with the central wake velocity $U_\infty(1-a)$ as is shown in figure 1.3, where $R_W - r$ is the distance measured from the wake edge, d is the distance between the discs, $U_\infty(1-a)$

is the central wake velocity and $U_\infty(1 - aF(r))$ the average velocity, where $F(r)$ is the Prandtl tip-loss function. It is worth noting that this model addresses the flow non-uniformities from the finite number of blades correcting the induced velocities which affect the loads indirectly.

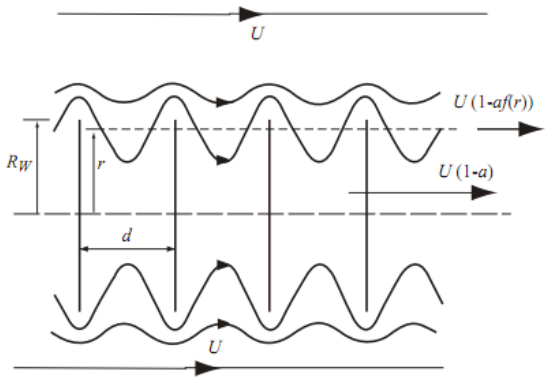

Figure 1.3: Prandtl's wake-disc model to account for tip losses [4].

In other words Prandtl's factor F expresses the ratio between the average value of a in the rotor plane and the induced velocity at the blade position a_B, $F = \frac{\bar{a}}{a_B}$ [4, 6]. This factor is applied in BEM equations for axial and angular momentum —see Appendix A—. Its behavior of some cases will be: whenever r is close to the rotor or whenever B approaches to infinity, $F \to 1$. In other words, Prandtl's model recovers the BEM theory when we have an infinite number of blades or far away from the tip. On the other hand, whenever $r = R$, $F \to 0$, which are reasonable suppositions. However, the Prandtl correction factor leads to a slight over-prediction of the loads is found at the tip of the blade ($r/R > 0.9$) when using two-dimensional data as an input to a BEM code. This is due to a three-dimensional effect of the blade geometry which is not taken into account in this correction.

It should be noted that Prandtl correction was done before computational tools and it relates the local blade velocity to the annulus averaged velocity. Nowadays, the assessment of Prandtl tip loss factor could be supported by calculations with a numerical full vortex wake methods carried out by softwares such as AWSM. This software was developed by ECN [10] and is based on a non-linear lifting line vortex wake model which calculates the induction factor in the rotor plane from the vorticity in the wake using Biot Savart law where the vorticity in the wake is trailed

from the rotor blades which are modeled as lifting lines. This software is used to probe the Prandtl tip loss factor behavior for different velocities.

Figure 1.4 show the comparison between Prandtl's factor computed by AWSM for different wind speed 10, 15 and 24 m/s and by means of equation (A.9). It is very interesting to note, over the tip blade region, that for wind speed of 10 m/s Prandtl tip loss factor computed analytically shows an under prediction of F, unlike for wind speed of 15 m/s where both computations show a good agreement; finally, for higher velocities, as is the case of 24 m/s Prandtl method compute a higher value of F compare with AWSM computations. It is worth noting how for low tip speed ratio the tip loss correction decrease significatevly. This results are obtained from MEXICO project and also showed in [11].

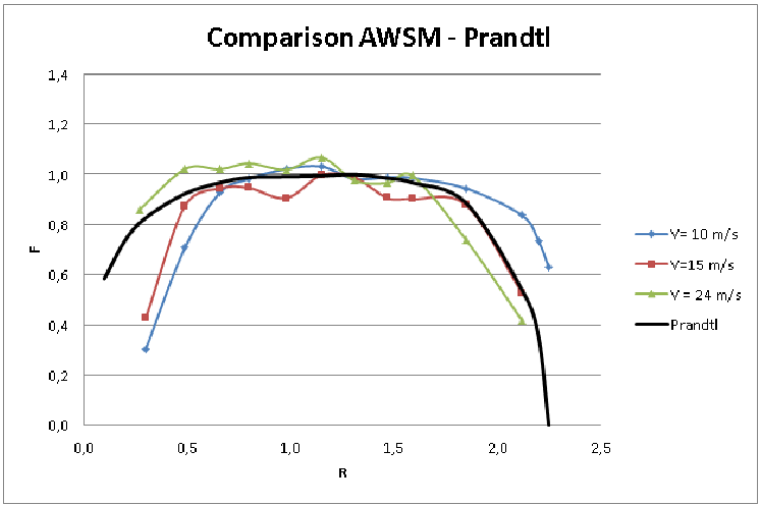

Figure 1.4: Prandtl's tip loss factor comparisson [4].

Results showed are taken from Model Rotor Experiments in Controlled Conditions (MEXICO) was a project carried out in 2006 by European Union where 10 institutes from 6 countries cooperated in doing experiments on a full scaled, 3 bladed wind turbine of 4,5 m diameter placed in The Netherlands. The result of this project was a large database of combined blade pressure distributions, loads and flow field measurements [12].

1.2.2. Other tip loss correction models

After Prandtl postulated his correction, several models have been developed in order to correct the tip loss effect, such as Wilson and Lissaman, de Vries, Mikkelsen et al, and more recently Shen, which are discussed in brief below [13].

Wilson and Lissaman [7] suggested that the mass flow through the rotor disc should be corrected in the same manner as the induced velocity is corrected with Prandtl's factor. Based on Prandtl theory taking the wake behavior as a succession of discs, and also considering as the ratio between the total induced velocity and the average of the velocity between the discs times the distance between them. They used the concept of circulation to reformulate the tip loss correction. As circulation is only caused by lift, they only take into account this force. Thus, the tangential interference factor is the same as for the Prandtl correction but, for the axial induction factor the mass flux and the induced velocity are corrected. However, this leads to a formulation in which the orthogonality condition between the induced velocity and the relative velocity at the blade element is not satisfied. In order to satisfy this condition, de Vries [8] introduces a model that corrects the mass flux in the tangential momentum equation and in the axial momentum equation.

Later on, Mikkelsen et al. [9] suggested a technique in which the induced velocities are first computed by the Navier-Stokes solver, after which they are corrected by means of the Prandtl tip loss function in the rotor before applying airfoil data.

1.2.3. Shen correction model

Shen et al. [6] presented an improvement with a more accurate tip loss correction. Their work is based on the statement that for a real rotor the axial velocity at the tip, where the tip vortex is generated and convected into a wake, is not zero. Thus, the inflow angle at the tip is not zero, either. They proposed to calculate their correction factor as the result of dividing the force coefficient by the two-dimensional data of the airfoil at the tip region in this way the correction is done directly on the loads. The model was done by comparing the normal forces computed by the different tip corrections with the NREL experimental data and for different wind speeds, as it is shown in figures 1.5 and 1.6.

The factor they found is very similar to that used by Prandtl but with the

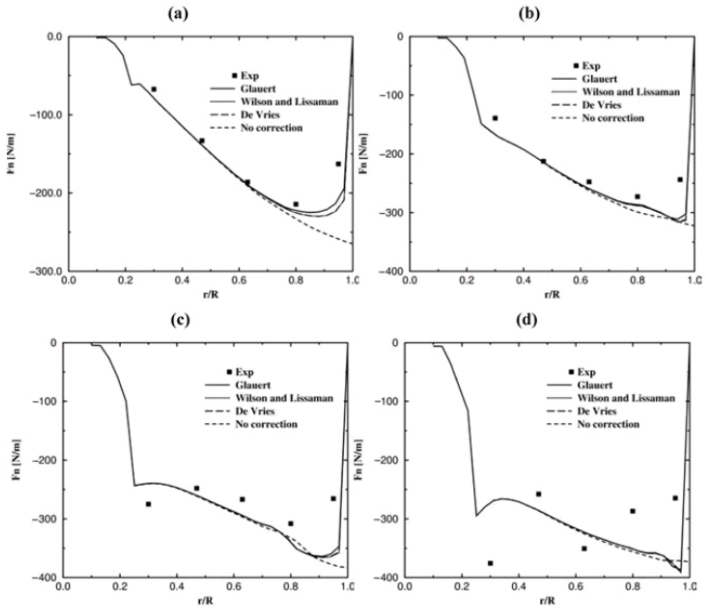

Figure 1.5: Comparison of normal forces computed with tip corrections and NREL experimental rotor [6].

addition of two new coefficients that take into account the effect of the tip speed ratio and enhanced the effect of the number of blades, by means of including a different correction factor called g namely

$$g = \exp[-c_1(B\lambda - c_2)], \tag{1.2}$$

where the coefficients c_1 and c_2 were computed experimentally, deriving and comparing the distribution of normal force near to the tip and then fitting the curve. This results in $c_1 = 0,125$ and $c_2 = 21$. This factor is introduced into the function F in the following way:

$$F(g) = \frac{2}{\pi}\cos^{-1}\exp\left[-g\frac{B(R-r)}{2R\sin\phi_R}\right]. \tag{1.3}$$

Looking at the data, one realizes that there is a much better achievement of the the results obtained by means of using this model. However, the agreement with the experimental data can be improved.

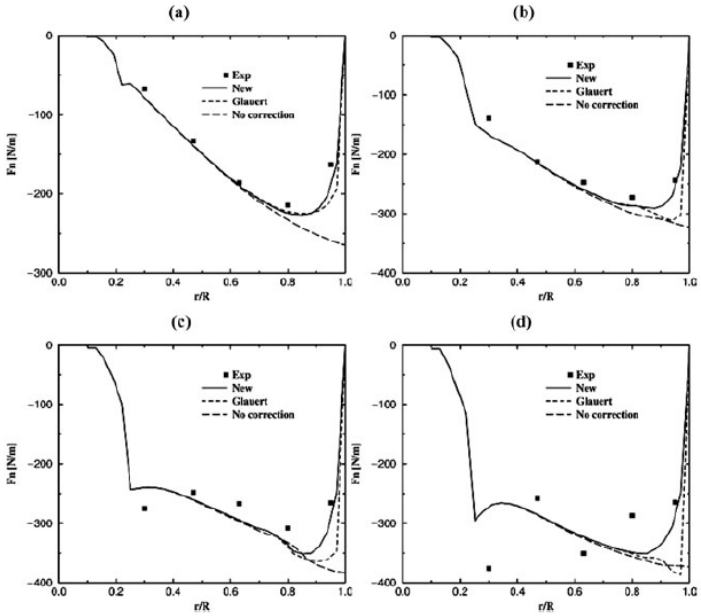

Figure 1.6: Comparison of normal forces computed with Shen tip correction and NREL experimental rotor [6].

Chapter 2

Data description and Analysis

Aimed to develop an empirical model, our work is based on data from different experiments, namely: the unsteady Aerodynamics Experiment (UAE) and the Enhanced field Rotor Aerodynamics Database (IEA). These experimental tests were done using three different turbines under different operational conditions. In this way, the present work will be supported by a wide range of parameters resulting in a corrected model ables to compute the tip loss effect and to correct the load distribution prediction over the blade.

This chapter describes the main characteristics of each project as well as the turbine used and the data obtained.

2.1. Unsteady Aerodynamics Experiment (UAE) NREL-NASA Ames

This project was conducted by the National Renewable Energy Laboratory of The United States of America and its main goal was to create a large database in order to quantify the behavior of a horizontal-axis wind turbines under different conditions.

This experiment sought to acquire aerodynamic and structural measurements on a full-scaled wind turbine located in a wind tunnel in order to obtain an environment free from large inflow disturbances. Several quantities, such as blade surface pressures as well as the inflow dynamic pressure, were measured at five span locations over the blade. The instrumentation used, data collection and processing will not be explained in this thesis because they are not relevant issues for the main topic

but they can be found in [14].

2.1.1. Test turbine description

The turbine used during this project was stall regulated, with full-span pitch control and a power rating of 20 kW. The tower was designed to obtain a hub height of 12.2 m. It was two bladed with twisted and tapered blades as shown in figure 2.1, with a 10 m diameter. The airfoil used was the S809. The two-dimensional data of this airfoil are shown in Appendix B.

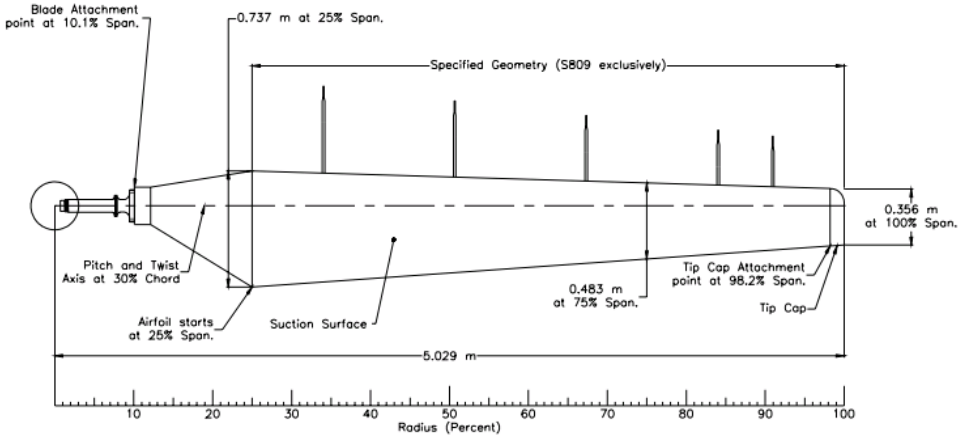

Figure 2.1: Blade dimensions [14]

For the goals of this thesis, just one sequence was taken in order to evaluate the tip loss effect. This sequence is called in the UEA report [14] *Test sequence H upwind baseline* where the test was carried out under conditions representative of a field operation. *Test sequence H* is a 30-second campaign under upwind conditions. The wind speed ranged from 5 m/s to 25 m/s. The blade tip pitch was 3 °. The rotation speed was fixed at 72 RPM and the blade span was $5,029$ m.

The blade shown in figure 2.1 was divided in 5 stations (at 30%,46%, 63%, 80% and 95% spanwise); in each station two measurements were taken: the dynamic pressure and the stagnation-point dynamic pressure. These measurements allow to derive a normalization pressure that was used to normalize each of blade surface pressures and in this way to compute the aerodynamic coefficients, such as the normal and the tangential forces, C_n and C_t, and the thrust and torque coefficients C_{TQ} and C_{TH}.

To calculate the aerodynamic coefficients shown in figure 2.2 for each span station, the pressure distribution for rotating blade was integrated in order to compute the aerodynamic coefficients. The torque and thrust coefficient were computed as function of C_n, C_t, the blade pitch angle β and local twist angle ϕ, to wit,

$$C_{TQ} = C_n \sin(\phi + \beta) + C_t \cos(\phi + \beta) \tag{2.1}$$

$$C_{TH} = C_n \cos(\phi + \beta) - C_t \sin(\phi + \beta). \tag{2.2}$$

In figure 2.2 are shown the angles involved in the aerodynamic analysis, such as the angle of attack α, the local inflow angle ϕ, and the pitch angle β as well as the aerodynamic coefficients (normal, tangential and thrust).

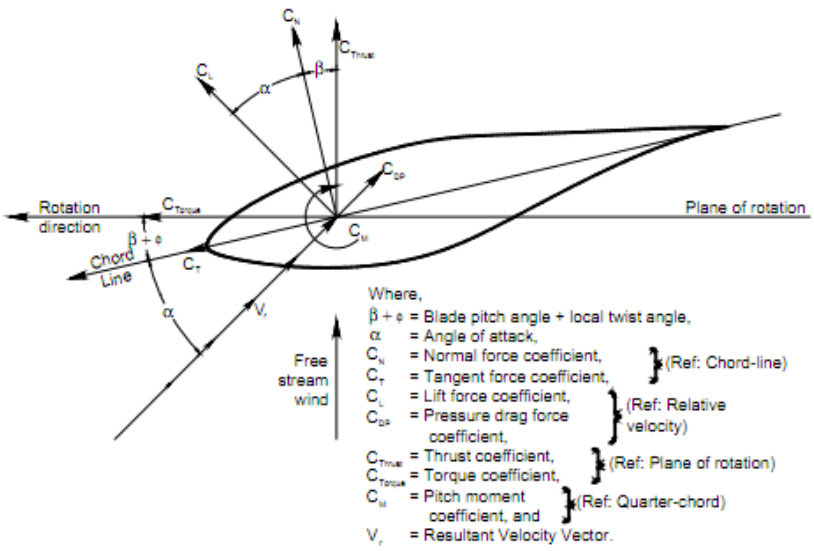

Figure 2.2: Local flow angle measurement convention [14]

To measure the angle of attack α, it was attempted to measure first the local inflow angle. Nevertheless, this measurement has to be corrected due to the effect of the upwash from the bound vorticity. Due to this the inverse BEM method has to be used to compute α. Besides these aerodynamic coefficients, other kind of data were measured, among others, rotation velocity, generator power, tunnel velocity, tunnel air density.

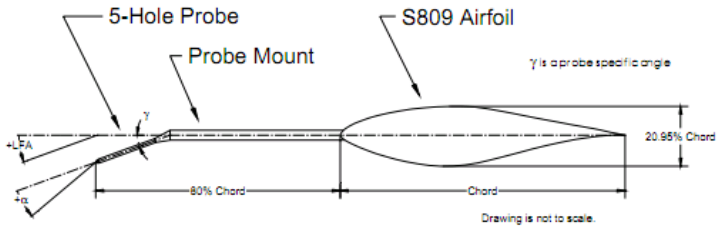

Figure 2.3: Probe to measure the local flow angle.

2.1.2. Data processing

The test was done for wind speed from 5 m/s to 25 m/s in time series of 10 min with a fix rotational speed of 72 rpm. From these data, was derived the figure 2.4 which shows the normal force coefficient C_n evolution over the blade span in order to have a first sight of the rotor behavior.

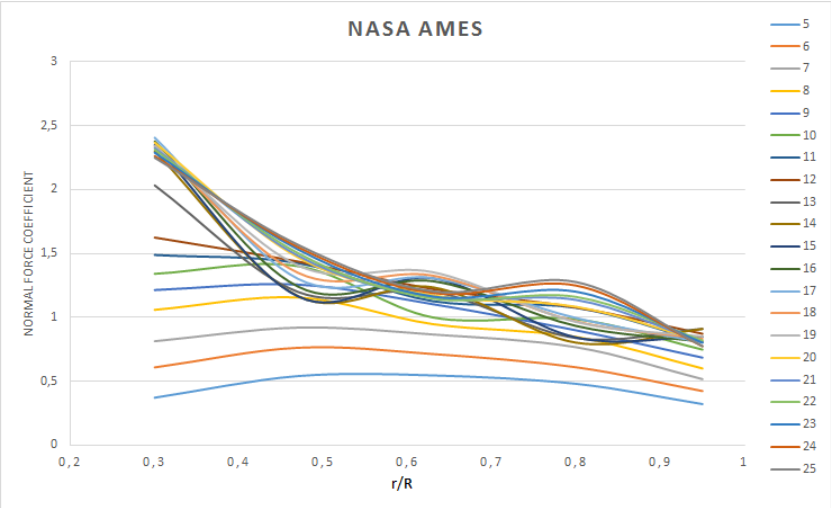

Figure 2.4: Normal force Coefficient vs. blade span-wise for different wind speeds in m/s.

The important fact that has to be noted in this figure is the clear reduction of the C_n over the outermost part of the blade (approx. 90%). It is also interesting the increasing of this value at the root of the blade (that means for 30% blade span) this is explained due to three dimensional effects as stall delay. It is worth mention that not all of these tests characterized the performance of a wind turbine, since they were done under fix rotational speed, generating high values of angle of attack

that under normal operational conditions are not achieved.

2.2. IEA: Enhanced Field Rotor Aerodynamics Database

This project was developed by different organizations from six different countries, collaborating in aerodynamic experimental programs on full scale horizontal axis wind turbines at field conditions. The aerodynamic quantities were measured likewise UEA NASA Ames project and as a result of this cooperation was created a database of measured data from each participant.

A total of five full scale test programs were coordinated but, for the purposes of this thesis, just two tests will be used. The complete performance of these projects will not be wide explained in this thesis but more information can be found in [15].

2.2.1. National Renewable Energy Laboratory (NREL),USA

Measurements for local flow angle and aerodynamic coefficients were taken at 34%, 51%, 67%, 81% and 91% blade span. The rotor is of 10 m diameter, three-bladed and downwind positioned, the blade span was 4.521 m and the profile used NREL S809 which two dimensional data will be found in Appendix B

This test was done in yawed and non-yawed sequences for different wind speeds and rotational speed. The C_n behavior over the blade is shown in figure 2.5.

It is easy to appreciate that the behavior under yawed and non-yawed conditions is pretty similar and it just depends of the wind speed. Moreover, as it was expected, over the tip of the blade the C_n value decrease.

2.2.2. RISO National Laboratory, Denmark

The wind turbine tested is 100 kW, three-bladed turbine, 19 m diameter turbine, with twisted and tapered blades. The hub height was 29.3 m, blade length: 8,2 m, profile blade length: 6.8 m root chord: 1.09 m, tip chord: 0.45 m and blade profile NACA 63n-2nn series which two-dimensional data will be found in Appendix C.

The measures of this project were mainly the aerodynamic forces over three segments of the blade (37%, 68% and 98%). These measures were taken under

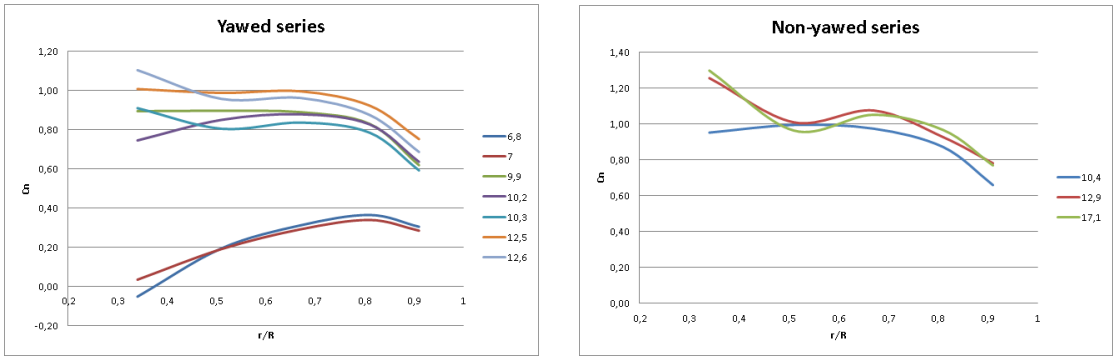

(a) **(b)**

Figure 2.5: NREL–C_n behavior over the blade for different wind speeds in (a) yawed condition and (b) non-yawed condition

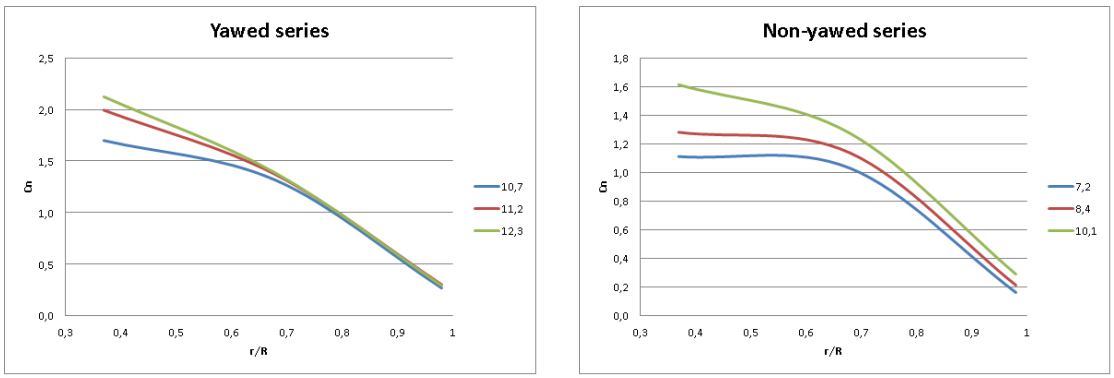

(a) **(b)**

Figure 2.6: RISØ–C_n behavior over the blade for different wind speeds in (a) yawed condition and (b) non-yawed condition

yawed and non-yawed conditions and for tip speed ratios between 2 and 5. The change of the C_n behavior is shown in figure 2.6 where is possible to see the change over the blade span. It is very important to note that in this case the blade geometry is not the same over its span because, as it was mention before, this blade is tapped which means that the airfoil use is not the same over the entire blade span.

In figure 2.6 is shown test series under yawed and non-yawed conditions for different wind speeds.

Chapter 3

New Model

As it was stated in the introduction, since the Prandtl theoretical correction, some other authors have attempted to develop a better solution of the problem of computing the load distribution over the blade. Nowadays, Shen's correction model is one of the most widely used. As a result of the literature revision, we believe that the existent corrections would improve their results if they would take into account parameters that might have some relevant effect into the tip loss phenomena, such as the chord.

This chapter is aimed to show the computations we have done in order to develop our proposed new correction model. Among others, this chapter displays the scheme followed to estimate the angle of attack required to process some data. At the end of this chapter, we present and develop the new correction model.

3.1. Angle of attack determination

The angle of attack is one of the most useful parameters in the aerodynamics field. It is defined in the two dimensional analysis as the angle between the chord and the undisturbed wind stream. Therefore, it is not extremely difficult to estimate it in a wind tunnel experiment, because the stream lines are aligned with the tunnel walls. However, this quantity is highly difficult to determine in a three-dimensional analysis because it is not possible to know a well-defined path for the undisturbed wind stream when it is not aligned with the wind tunnel walls. This is enhanced by the fact that it is not possible to use the undisturbed wind vector far from the rotor because it does not include the induced velocities caused by the wake present behind the rotor [15, 16].

The projects used in this thesis have developed different techniques for measuring an accurate angle of attack as well as the local inflow angle ahead of the airfoil. In general, it is used a five hole pitot probes as the measuring device shown in figure 3.1, where it is easily noted that the angle of attack is not the angle measured. To obtain the angle of attack, the up-wash induced velocity by the bound vorticity should be subtracted from the angles measured. Figure 3.1 also represents the velocity triangle where the angle of attack is related with the airfoil chord, the effective velocity W, the axial velocity and rotational velocity components $(V - U_i)$ and $(\omega \cdot r)$.

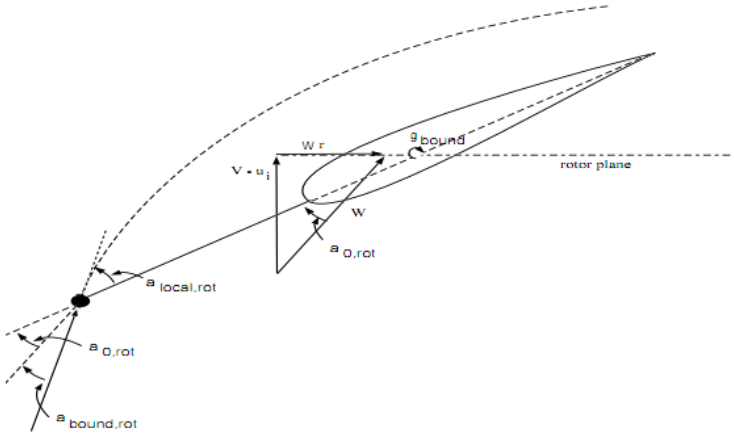

Figure 3.1: Angle of attack measurement in wind tunnel [14]. Here $a_{local,rot}$ is the local inflow angle measured by the device, $a_{0,rot}$ is the angle of attack in a rotating wind turbine and $a_{boundrot}$ is the up-wash angle induced by the bound vorticity.

In what it concerns with the NREL project, they have developed a correction of the angle measured in order to compute the angle of attack [17]. This correction is given by the following relation:

$$\alpha = -5,427 \times 10^{-5} \cdot \alpha_m^3 + 6,71 \times 10^{-3} \cdot \alpha_m^2 - 0,8293, \tag{3.1}$$

where α is the up-wash corrected angle of attack (deg), α_m is the local flow angle measurement. The data from UEA in the test sequences do not contain the local flow angle as a measurements. Thus, it has to be estimated by one of the different methods aimed to compute the angle of attack. These methods are: a) the inverse blade-element momentum method, b) the averaging technique and c) the inverse

free wake method [18], d) Computationa fluid mechanics CFD [19] and recently published experimental techniques such as PIV measurements [20].

3.2. Inverse BEM

The inverse BEM method is a very appropriate methodology in this case, because it employs the normal and tangential force measurements on the blade sections and these data are available from the experiment. The method consists in using the equations for the axial and tangential forces iteratively to establish the axial and tangential induction factors [3]. By means of the velocity triangle at the blade, the angle of attack can be found as a function of the local inflow angle.

The BEM method allows to know the relation between the normal force and the thrust as well as the relation between the tangential force and the torque. Those relations are the following:

$$dT = BF_N\,dr \quad \text{and} \quad dM = rBF_T\,dr. \tag{3.2}$$

Here dT is thrust, dM the infinitesimal torque, B is the number of blades, r is the radial distance to the center of the rotor, dr an infinitesimal piece of blade and F_N and F_T are the normal and tangential forces. It is also known that thrust and torque are defined as

$$dT = 4\pi r\rho V_0^2 a(1-a)dr \quad \text{and} \quad dM = 4\pi r^3\rho V_0\omega(1-a)a'dr. \tag{3.3}$$

where ρ is the density of the air, ω is the angular velocity of the rotor, V_0 is the free stream wind speed and a is the induction factor. Figure 3.2 shows the aerodynamic forces over the blade. Since the inflow angle ϕ is now known, it is possible to calculate the angle of attack α which depends of the pitch of the airfoil as well.

We introduce an iterative procedure. The initial data are: the wind velocity U_∞, the angular velocity of the rotor Ω, the blade length r, the number of blades B, the chord c and the coefficients c_n and c_t. We use that the angle of attack is given by the expression [3]:

$$\tan\alpha = \frac{U_\infty(1-a)}{\Omega r(1+a')}, \quad \text{for the lift coefficient} \quad c_l = c_n\cos\alpha - c_t\sin\alpha;$$

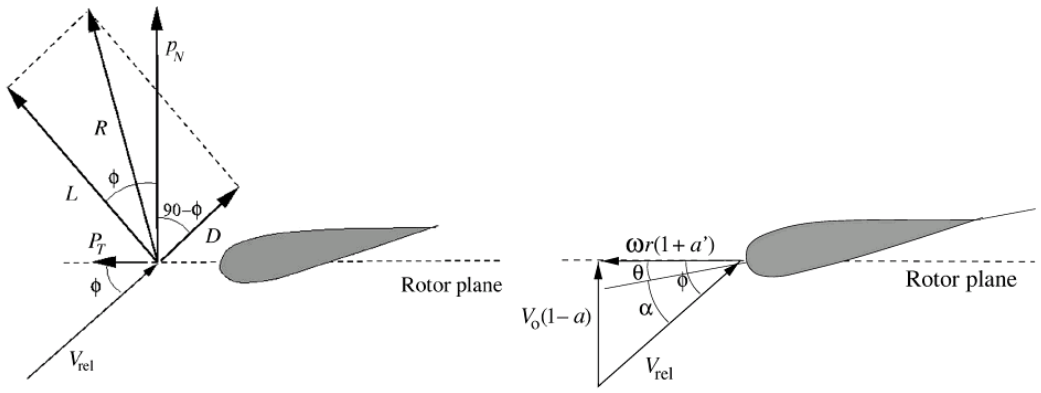

Figure 3.2: Local forces and velocities at the blade [1].

and the expression for the coefficients:

$$a = \frac{1}{1 + \frac{4\sin^2\alpha}{\sigma' c_l \cos\alpha}} \quad \text{and} \quad a' = \frac{1}{\frac{4\cos\alpha}{\sigma' c_l} - 1},$$

where $\sigma' = Bc/2\pi r$. The procedure consists in taking some values for a and a' (say, for instance 0.3 and 0.4), and then compute α. The value of the angle of attack allows to compute a new factors a and a' and so on. It converges very fast.

The test sequences contain measurements of the normal and tangential force coefficients. Thus, it is easy to derive ϕ and α, clearing from (3.4) the forces and let them as function of their respective coefficients

$$C_n = \frac{F_N}{\frac{1}{2}\rho V_{rel}^2 c} \quad \text{and} \quad C_t = \frac{F_T}{\frac{1}{2}\rho V_{rel}^2 c}. \tag{3.4}$$

3.3. New correction model

As it was mentioned, Prandtl factor F corrects the assumption of an infinite number of blades used in BEM method. This factor is multiplied by the rotational and axial forces and in this way a new (corrected) induction factors (axial and tangential) are derived. This can be understood as a correction factor of the rotational effects over the two dimensional data.

It is correct to assume that the two dimensional data do not include any loss while the experimental data have a loss due to rotational effects. Thus, knowing the two dimensional aerodynamic coefficients and the experimental angles of attack,

it should be easy to compare them to the experimental measurements, because we have the expressions:

$$C_n^{exp} = FC_n \quad \text{and} \quad C_t^{exp} = FC_t, \tag{3.5}$$

where F is the correction factor, C_n and C_t are the two dimensional data and C_n^{exp} and C_t^{exp} are the experimental data (which contain the three-dimensional rotational effect).

The Shen corrected model discussed previously (see subsection 1.2.3) includes the rotational effects, so that according to the expression (3.5) it is possible to correct the two dimensional data with the F factor and obtain, in this way, new three dimensional data comparable with the experimental measurements.

In this section we will develop a new correction factor to be added into the existing Shen correction model when the chord distribution will be the only new parameter to integrate in the aforementioned correction.

In this part we will focus just in the 95% blade span, because as we already mention the tip loss effect occurs mainly at the tip region of the blade. Before that 95%, the corrected two dimensional data and the experimental measurements must have more less the same value since there is not effect from the tip. This assumption is consequence of the exponential behavior of the correction factor and the fact that in the root of the blade F takes values close to one. In other words, in this region the two-dimensional data do not suffer any correction because there is not stall at the root caused by tip loss.

The correction model has to follow. First of all, in the case of a rotor with an infinite number of blades or in the case of a rotor running at an infinite tip speed, there must be no correction, then $F = 1$. Second, unlike the previous conditions, when approaching to the end of the blade, the correction should make the forces tend to zero since at this point the effect of the vortex circulation on the induced velocity factors make them increase.

Once the two-dimensional data are corrected by means of the Shen's model, and compare them to the experimental measurements, one can compute the error due to Shen's. Moreover, it is possible to know in which way it is possible to improve this model, assuming that the corrected data include the rotational effects, that the experimental measurements already have.

For UEA project the comparison among different data is presented in figure 3.3. It exhibits a very good agreement between the corrected two dimensional and the experimental data for angles of attack from 4 ° to 5 °.

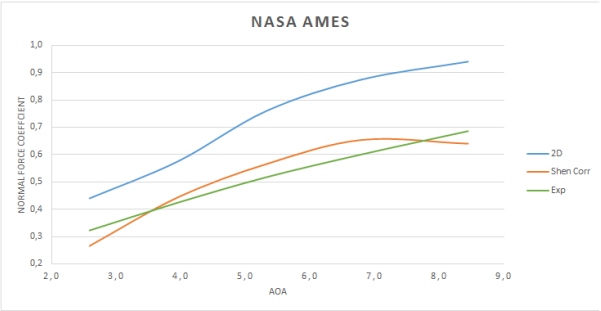

Figure 3.3: Comparison of two dimensional, corrected and experimental data for UEA project.

In the case before it was expected a good agreement between corrected and experimental data given that Shen et al. developed their work based on these data. The same comparison was done for the other two tests. In these other cases the agreement between the corrected and the experimental data is not longer as good as it was for the case of EUA NASA Ames test.

Due to the difference between the experimental data and Shen's results it seems plausible that an improvement of Shen's correction could be performed. Besides, it is possible to presume that as we thought not only the tip speed ratio and the number of blades must be in the correction. More parameters must be analyzed to find the shape that a new correction can take. Then, we compute the difference between the experimental and the corrected two dimensional data, to wit, $\frac{C_n exp}{C_n corr}$.

As a consequence of the above discussion we obtained a new model which looks like follow:

$$F_{\text{new}}(g, s, \sigma) = F(g)m(s, \sigma) \quad \text{where} \quad F(g) = \frac{2}{\pi}\cos^{-1}\exp\left[-g\frac{B(R-r)}{2R\sin\phi_R}\right].$$

Here g is the function introduced by Shen, which only depends on the number of blades and tip speed ratio. The new function $m(s, \sigma)$ exhibits also an exponential behavior and assumes the following form:

$$m(s, \sigma) = 1 - s^{c_3}\exp(-c_4\sigma), \tag{3.6}$$

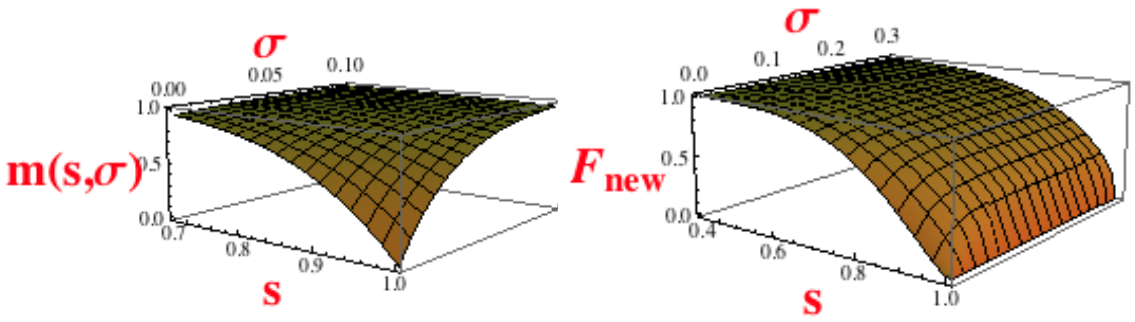

(a) Correcting factor $m(s, \sigma)$ **(b)** Profile of the function $F_{\text{new}}(g, s, \sigma)$

Figure 3.4: New model behavior

where $s = \frac{r}{R}$ and σ is the solidity ($\frac{Bc}{2\pi r}$). Making use of a curve fit, we obtain that $c_3 = 8$ and $c_4 = 34.2$ are the coefficients which reduce the observed error.

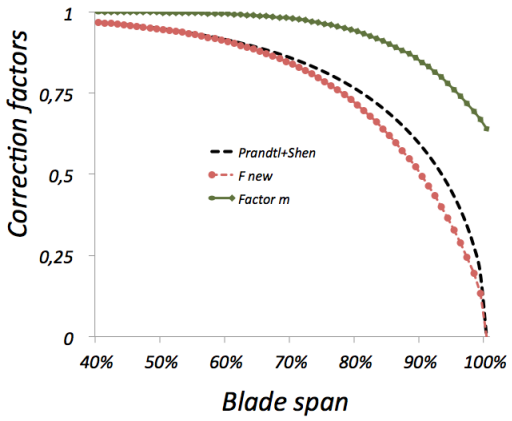

Figure 3.5: Profile of the function $F_{\text{new}}(g, s, \sigma)$, F and $m(s, \sigma)$ for a rotor with three-blade rotor and an inflow angle of 18° and a solidity of 0,15.

It is clear from figure 3.4 that our extremal cases are:

$$m(1, 0) = 0 \quad \text{and} \quad m(s, \sigma \to \infty) = 1.$$

These cases can be read in two ways. If the solidity is zero, there is no chord (there is no blade at all) and therefore there is no power to loss. If the solidity tends to infinity the number of blades or the chord is infinitely large; in both cases there is no tip loss. These are clearly reasonable assumptions.

The model we have developed was constructed in order to correct the model by Shen only in the region in which it displays incorrect values, that is, when the

loads are computed near to the tip of the blade. In the other cases, the model does not play any role. This situation is better shown in the figure 3.5 where our model corrects the Shen's profile only when the blade span is bigger than 75% and lower than 98%. In the inner region the model reduces the already mentioned over prediction of the loads resulted from applying the Shen model.

Chapter 4

Results and conclusions

Previously in this thesis, we have discussed the models existing to date for correcting the BEM theory in what it concerns to the tip losses. We have analyzed the data of three different wind turbines and concluded that an improvement can be carried out if we take in consideration the chord of the tip. Our main goal has been to produce an empirical description of this phenomena. This section is aimed to test the model in a different project. Therefore, the main goal of this chapter is to evaluate the performance of the new correction, comparing its behavior as well as the model developed by Shen et al. with the experimental data. At the end of this chapter, we discuss the conclusions of this work and offer some recommendations for future work.

4.1. Results

The new correction model was tested and compared with the data from the test sequences with axial flow in NREL and RISØ projects, under different conditions as yaw, pitch angle, wind speed and tip speed ratio. The comparisons exhibit in figures 4.1, 4.2 and 4.3 show a remarkable performance of the proposed model, whose error with the experimental data is much lower than the error produced by Shen's model.

Figures 4.1 and 4.2 show the comparison for NREL data under yawed and non-yawed conditions, respectively. In the case of non-yawed conditions the new model does not improve the results obtained with Shen's model. It is clearly remarked the cases when Shen's results are accurate the new model does not have a good agreement with experimental data.

In the case of yawed conditions campaign showed in 4.2 the new correction

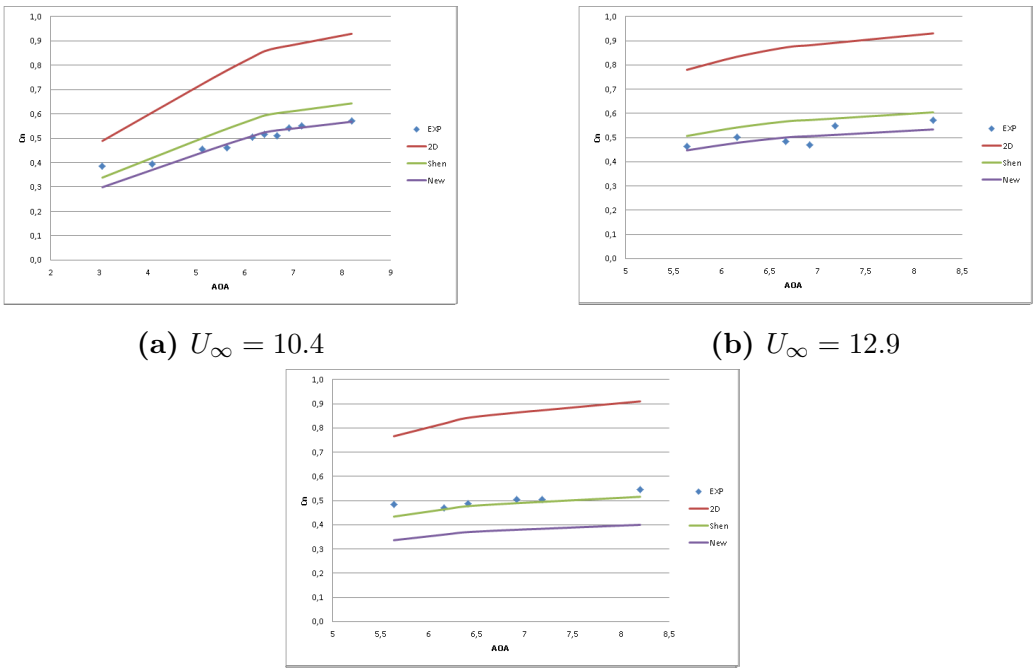

(a) $U_\infty = 10.4$ **(b)** $U_\infty = 12.9$

(c) $U_\infty = 17.1$

Figure 4.1: Comparison of the C_n behavior with the new correction with Shen correction and two-dimensional and experimental data. NREL-Non-yawed campaigns

present a much better behavior improving Shen's results, specially for the cases of higher wind speed, in other words, lower tip speed ratios.

In the same way, for RISØ cases there is a very good agreement between the new correction and the experimental data for wind speeds of 7.2 m/s and 10.1 m/s. These results will be shown in figure 4.3 It is important to recall that due to this model was developed in an empirical way it is difficult to explain some of the results obtained as far there is not a physical model.

4.2. Conclusions

In this work we have studied in depth the tip loss phenomena. We have investigated the results obtained from Shen's correction which is nowadays the model most used and compare them with experimental values. Our main goal has been to introduce other parameters which could affect the tip loss effect. We found that, for instance, the geometry of the airfoil plays an important role in the physics in-

volved in this effect and in this sense the chord is an important variable in the phenomenology of the power losing. There are three main conclusions:

- Our new model corrects some disagreements between the prediction of the model by Shen and the observed values, including the solidity (a function of the chord) as a new parameter. This results in a remarkable improvement of the load prediction especially for low tip speed ratios.
- Taking in consideration extremal cases (a length of the chord close to zero, for instance), it is possible to produce a profile of the connection between the chord and the tip loss. We have proposed an exponential decay law.
- In any case, it is clear that the geometry of the tip influences the airflow crossing the blades. In this sense, future corrections of the Prandtl, Shen and our model itself, has to deal with the task of comprehend this connection.

Of course, a more physical analysis shall yield a complete mathematical description of the connection between the geometry of the chord and the tip loss phenomena, but we hope that this empirical analysis is a first step in the right direction. It would be interesting define the different parameters involved in this effect and the way that they affect the aerodynamical behavior of the wind turbine.

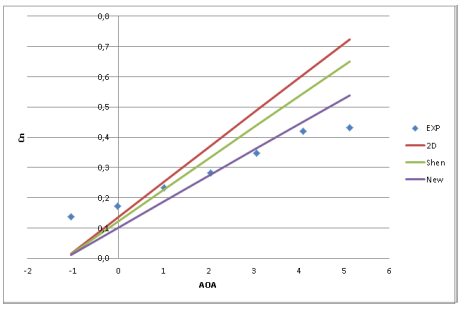

(a) $U_\infty = 7.0$

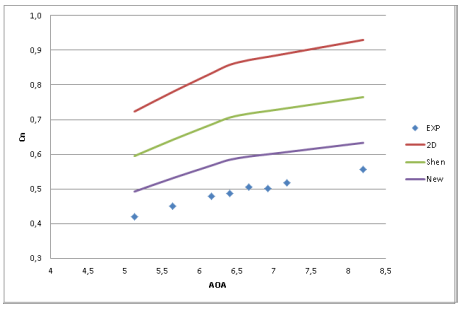

(b) $U_\infty = 9.9$

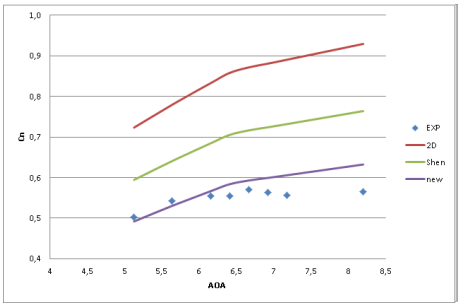

(c) $U_\infty = 10.2$

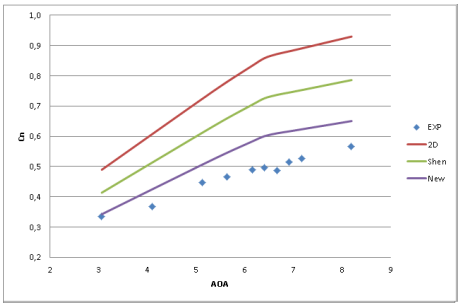

(d) $U_\infty = 10.3$

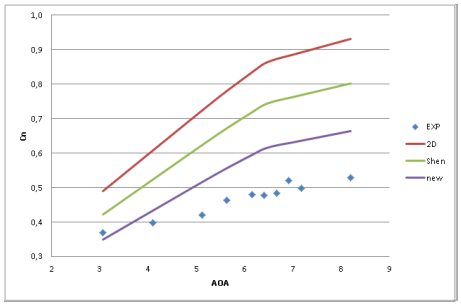

(e) $U_\infty = 12.6$

Figure 4.2: Comparison of the C_n behavior with the new correction with Shen correction and two-dimensional and experimental data. NREL– Yawed campaigns

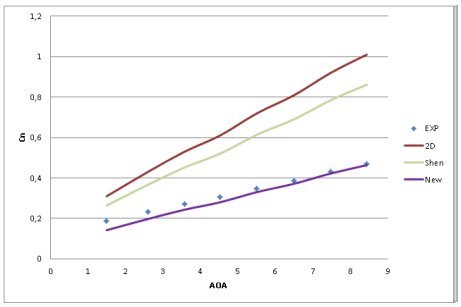

(a) $U_\infty = 7.2$

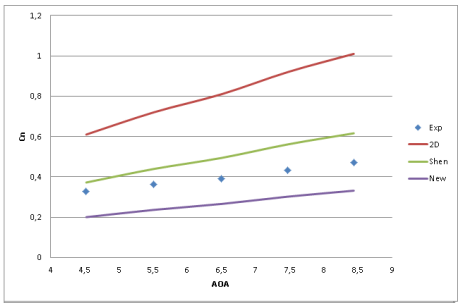

(b) $U_\infty = 8.4$

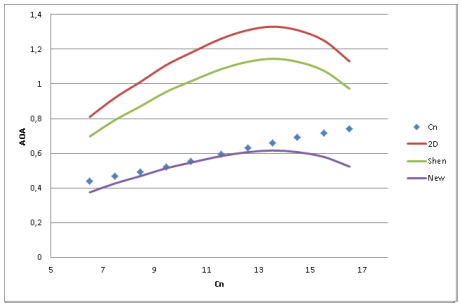

(c) $U_\infty = 10.1$

Figure 4.3: Comparison of the C_n behavior with the new correction with Shen correction and two-dimensional and experimental data. RISØ– Non-Yawed campaigns

Appendix A

Theoretical background

This chapter provides a brief theoretical survey in aerodynamics, concepts needed to develop the model for the tip loss effect correction. The first three sections introduce some basis doing a brief mention of the one-dimensional momentum theory, blade element theory and vortex system. The last section is aimed to explain the blade element momentum model.

A.1. Two dimensional aerodynamics

A first approximation for understanding the flow passing over the blades is done by a two-dimensional analysis. The first statement for this analysis is that the flow is confined into a plane and then is projected outward a blade of infinite span. This allows to analyze and understand the basic principles behind the aerodynamic behavior in a wind turbine.

$$P = \vec{F} \cdot \vec{u} \tag{A.1}$$

where P is power, $\vec{F}$ is a force vector and $\vec{u}$ is the blade speed.

The power comes from the force of the air concentrated at the rotor disc. As power depends proportionally to the force, one of the goals of wind turbine modeling is to increase and control its magnitude and distribution. The force vector is produced for the flow passing over the blades. It is decomposed in two components: one perpendicular and another parallel to the incoming flow direction. These components are lift and drag, respectively. To describe completely the force system in a blade it should be introduced a moment around a point in the airfoil which is positive when it tends to turn the airfoil clockwise.

In order to describe the characteristics of a wide range of wind turbines those forces are dimensionless resulting in the lift, drag and momentum coefficient, which at the same time derive in normal, tangential and torque coefficients.

A.2. Three dimensional analysis

Unlike the section above, in this case the blade is no longer a wing with infinite span. Now, it is a finite length wing with different kinds of airfoils as cross sections. The air flow splits in two sides of the airfoil is found, at the tip the streamlines flowing over and under the airfoil will be deflected inwards and outwards. Therefore, at the trailing edge there is a jump in the tangential component of the velocity [1] yielding to a sheet of vorticity in the wake behind the blade called *free vortices*.

A.3. One dimensional momentum theory

The one dimensional momentum theory is based on the assumption that the rotor is an ideal disc, which means that it is considered frictionless and without rotational component in the wake.

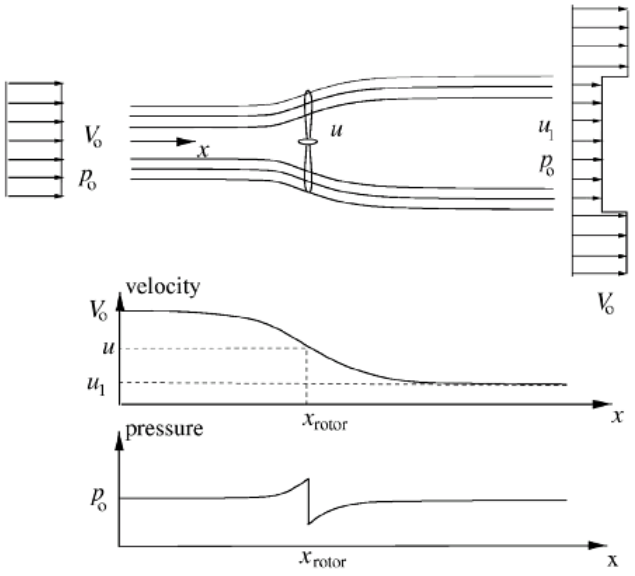

Figure A.1: Actuator disc.

Shown in Figure A.1 is the actuator disc where it is possible to see the drop in the velocity at the rotor plane. Then, one can define the axial induction factor a, as the decrease in wind velocity between the free stream and the rotor plane. The induced velocity at the rotor is usually referred as $U_1 a$ in this case the velocity at the rotor is a combination of the free stream and the induced velocity. Where the axial induction factor increase from zero (far away from the rotor)[21].

Due to the assumption of an ideal rotor, it is possible to derive relations between the velocities U_∞, the thrust T and the power P, [1] yielding:

$$T = 2a\rho U_\infty^2 (1-a)A \tag{A.2}$$

$$P_{avail} = \frac{1}{2}\dot{m}U_\infty^2 = \frac{1}{2}\rho U_\infty^3 A, \tag{A.3}$$

where ρ is air density, a induction factor, A the rotor disc area, $\dot{m}$ is the mass flow and P_{avail} is the power available in the air.

A.3.1. Wake rotation and Vortex system

In a real rotor there is rotation in the wake, contrary to what was assumed in previous section; then, the effect of the wake should be noted. In every blade of a wind turbine a vortex sheet is generated in the trailing edge. Due to the rotation of the blade the tip describes a circular path. Then, the free vortices generated on the tip form a helix in the wake behind the rotor. And the root vortices follow a linear path along the rotor axis, as it is shown in figure A.2.The generation of rotational kinetic energy in the wake results in a loss of energy extraction by the rotor. This energy in the wake will be higher if the generated torque is higher [3, 21]. Thus, turbines running at low speed ratios and high torque will experience more wake rotation losses.

The inclusion of angular velocity component provided by the wind to the rotor can be express as an angular induction factor defined as $a' = \frac{\omega}{2\Omega}$. Thus, the induced velocity will consist in two components one axial Ua and one component in the rotor plane $r\Omega a'$.

Deriving into a different equation of power applied to an infinitesimal control volume with thickness dr.

$$dP = 4\pi\rho\omega^2 U_\infty a'(1-a)r^3 dr. \tag{A.4}$$

Knowing that the power comes from the air force concentrated at the rotor disc, as equation (A.1), it can also be defined by

$$P = FU_d = 2\rho A_d U_\infty^3 a(1-a)^2. \tag{A.5}$$

The power coefficient C_p an be defined as: $\frac{P}{P_{avail}}$; therefore, $C_p = 4a(1-a)^2$. The maximum power that can be obtained from a wind turbine is derived by the well known Betz limit [1, 4] which states that a theoretical maximum of $C_p = \frac{16}{27}$ exist for $a = \frac{1}{3}$ and $a' = \frac{a(1-a)}{\lambda^2\mu^2}$. The resulting axial and tangential velocities are given by the expressions:

$$V_a = (1-a)U_\infty \quad \text{and} \quad V_{rot} = (1-a')\omega r. \tag{A.6}$$

then,

$$\phi = \tan^{-1}\frac{V_a}{V_{rot}} \qquad \alpha = \phi - \theta. \tag{A.7}$$

where θ is the pitch angle of the airfoil.

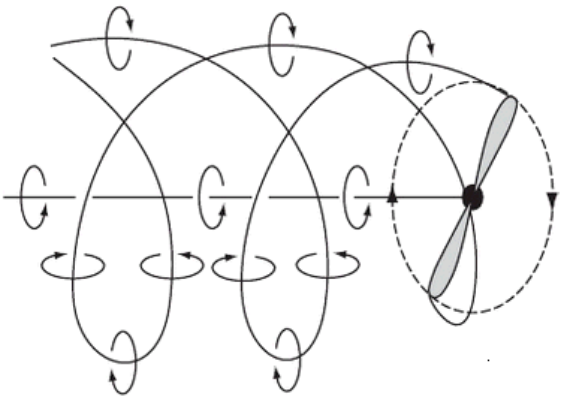

Figure A.2: Helical trailing tip vortices [4]

A.4. The blade element momentum Method (BEM)

This method works based on a stream tube as a control volume whose shape is given by an annular element that it is the rotor with a cut made at a radial distance r and wide dr. Basically, BEM method seeks to divide the blade into small pieces where can be compute the aerodynamic forces taking into account two main assumptions [1, 22].

1. Radial independence. The parameters used and calculated at a certain span position depend only of the local aerodynamics forces at the same position. This does not affect the other elements.

2. The rotor has an infinite number of blades. Thus, the blade's force acting on the flow is constant in each element.

From the second assumption it is possible to infer that since there is an infinite number of blades on the rotor, then every particle of fluid passing through the rotor interacts with the blades. But, evidently this is not a real situation, because a real wind turbine has a finite number of blades and hence some particles of fluid will interact with the blades and other ones will not.

This have an important effect in the blade since the loss of momentum by a particle depends on the interaction with the blades. Consequently, the axial induced velocity will change at any moment and therefore the axial momentum of the flow and the forces on the blade will change, as well.

Finally, the BEM method calculates these induction factors and thus the loads distribution on a wind turbine, to wit,

$$a = \frac{1}{(\frac{4\sin^2\phi}{\sigma C_n}) + 1} \quad \text{and} \quad a' = \frac{1}{\frac{(4\sin\phi\cos\phi)}{\sigma C_t} - 1}. \tag{A.8}$$

A.5. Prandtl tip loss factor

The importance of the components of the induced velocity among others is that they depend of the position on the blade, this means, they change all over the blade span. That is why the first model done in order to correct the tip loss effect was an attempt to asses the value of the induced velocity at the tip.

Prandtl tip loss factor F express the ratio between the average induced velocity and the induce velocity at the blade position

$$F = \frac{\bar{a}}{a_B}$$

where a_B is the axial interference factor at the blade section and $\bar{a}$ is the average and local axial factor. Now, it is worth to note that for a rotor with infinite number of blades, a_B and $\bar{a}$ become identical. Then Prandtl attempt is to introduce the tip

loss factor as a correction to the induce factors a and a' using F through the axial and angular momentum equations respectively.

Prandtl based his analysis on the fact that the circulation on a real rotor tends to zero exponentially when it is proximate to the blade tip. Close to the rotor center, it is possible to analyze this part as a continuos disc; but, as far as the analysis is done close to the tip the actuator disc model is not longer applicable. This analysis is possible since, the relation between the blade surface and the rotor surface is given by

$$\frac{Bc}{2\pi r}$$

where B is the number of blades, c is the chord of the blade and r the local radius. This relation between blade and rotor area is the so-called *solidity* (σ). Now, as this relation depend of the number of blades it is clear that the tip loss will change as smaller the number of blades is.

Thus, to correct the discrete number of blades Prandtl derived his correction factor computed as:

$$F = \frac{2}{\pi}\cos^{-1}(e^{-f}) \tag{A.9}$$

where

$$f = \frac{B}{2}\frac{R-r}{r\sin\phi}$$

B is the number of blades, R is the overall radius of the rotor, r is the local radius and ϕ is the flow angle.

Appendix B

Two dimensional data for S809 Airfoil

Here it is shown the two-dimensional aerodynamical coefficients for the S809 airfoil.

α	C_l	C_d
$-2,23$	$-0,600$	$0,006$
$-0,16$	$0,156$	$0,004$
$1,84$	$0,369$	$0,006$
$3,88$	$0,571$	$0,008$
$5,89$	$0,755$	$0,009$
$7,89$	$0,860$	$0,017$
$8,95$	$0,887$	$0,024$
$9,91$	$0,869$	$0,035$
$10,90$	$0,868$	$0,039$
$12,00$	$0,894$	$0,048$
$12,90$	$0,938$	$0,061$
$14,00$	$0,929$	$0,074$
$14,90$	$0,908$	$0,080$
$16,00$	$0,912$	$0,106$
$17,00$	$0,655$	$0,271$
$18,00$	$0,588$	$0,265$
$19,00$	$0,587$	$0,281$
$20,00$	$0,597$	$0,299$

α	C_l	C_d
$22,00$	$0,603$	$0,326$
$24,00$	$0,647$	$0,375$
$26,00$	$0,683$	$0,419$
$28,10$	$0,745$	$0,482$
$30,00$	$0,824$	$0,560$
$35,00$	$1,050$	$0,817$
$40,00$	$1,140$	$1,030$
$45,00$	$1,200$	$1,260$
$50,00$	$1,120$	$1,380$
$55,00$	$1,170$	$1,700$
$60,00$	$1,080$	$1,870$
$65,00$	$0,940$	$1,980$
$70,00$	$0,857$	$2,190$
$74,90$	$0,666$	$2,170$
$79,90$	$0,472$	$2,210$
$84,80$	$0,356$	$2,320$
$89,90$	$0,142$	$2,090$

Appendix C

Two dimensional coefficients for NACA Series 63nn-2nn

Here it is shown the two-dimensional aerodynamical coefficients for the airfoils NACA Series 63nn-2nn.

[c] t/c	12%	15%	18%	21%	25%
α					
0	0,156	0,156	0,156	0,156	0,156
2	0,365	0,365	0,365	0,365	0,366
4	0,569	0,569	0,569	0,569	0,570
6	0,768	0,768	0,768	0,768	0,759
8	0,962	0,952	0,934	0,925	0,906
10	1,149	1,121	1,085	1,040	0,985
12	1,285	1,222	1,160	1,079	1,007
14	1,331	1,260	1,172	1,075	0,995
16	1,185	1,150	1,108	1,048	0,970
18	0,753	0,962	1,004	1,021	0,971
20	0,697	0,822	0,948	0,992	0,987
25	0,943	0,959	0,968	0,977	0,986
30	1,032	1,039	1,039	1,039	1,047
40	1,108	1,114	1,120	1,126	1,131
50	1,159	1,159	1,159	1,159	1,159
60	1,170	1,170	1,170	1,170	1,170
70	1,190	1,190	1,190	1,190	1,190
80	1,224	1,224	1,224	1,224	1,224
90	1,307	1,307	1,261	1,261	1,261

Bibliography

[1] Hansen M., *Aerodynamics of wind turbines*, Copenhagen: Technical University of Denmark, 2000.

[2] Hansen M., Sørensena J., Voutsinasb S., Srensenc N., Madsenc D., "State of the art in wind turbine aerodynamics and aeroelasticity", *Progress in Aerospace Sciences*, 2006; 42: 285-330.

[3] Manwell J. F., McGowan J. G., Rogerts A. L., *Wind energy explained:Theory, design and application*, Chichester: John Wiley and Sons, 2002.

[4] Burton T., Sharpe D., Jenkins N., Bossanyi E., *Wind Energy Handbook* Chichester: John Wiley and Sons, 20011.

[5] Prandtl L., Betz A., *Vier Abhandlungen zur Hydrodynamik und Aerodynamik*, Göttingen: Universitätverlag Göttingen, 2010 [1927].

[6] Shen W.S. et al., "Tip loss corrections for wind turbine computations", *Wind energy*, 2005; 8: 457-475.

[7] Wilson R.E., Lissaman P.B.S., *Applied aerodynamics of wind power machines*, Oregon: Oregon State University Repost NSF/Ra/N-741113, 1974.

[8] De Vries O., "Fluid dynamic aspects of wind energy conversion", AGARD Report AG-243. 1979: 1-50.

[9] Mikkelsen R., Sorensen J.N., Shen W.S., "Modeling and analysis of the flow field around a coned rotor", *Wind energy*, 2001; 4: 121-135.

[10] Boorsma K., Grasso F., *ECN Aero Module Manual*, Peten: ECN, 2002.

[11] Schepers J.G., Boorsma K., Bon A., Kim C., Cho T., *Results from Mexnext: Analysis of detailed aerodynamic measurements on a 4.5 m diameter rotor placed in the large German Dutch wind tunnel DNW*, Peten: ECN, 2011.

[12] Shepers et al., *Final report of the IEA Task 29, MExnext (Phase 1):Analysis of Mexico wind tunnel measurements*, Peten: Energy Research Center of The Netherlands – ECN, 2012.

[13] Clifton-Smith M.M., "Wind turbine blade optimisation with Tip loss corrections", *Wind Engineering volume*, 2009; 33: 477-496.

[14] Hand M.M. et al., *Unsteady Aerodynamics Experiment Phase IV wind tunnel test configurations and available data campaigns*, National Renewable Energy Laboratory, NREL/TP-500-29955, 2001.

[15] Schepers J. G., *Engineering models in wind energy aerodynamics: Development, implementation and analysis using dedicated aerodynamic measurements*, TUDelft, PhD Thesis, 2012.

[16] Yang H., Shen W., Sørensen J. N., Zhu W., "Investigation of Load Prediction on the Mexico Rotor Using the Technique of Determination of the Angle of Attack", *Chinese Journal of Mechanical Engineering*, 2012; 25: 506-514.

[17] Shepers et al., *Final report of the IEA Annex XVIII: Enhanced Field Rotor Aerodynamics Database. ECN-C-02-016*, Peten: Energy Research Center of The Netherlands – ECN, 2002.

[18] Shen. W. S., Hansen M. O. L., Sorensen. J. N., "Determination of the angle of attack on Rotor blades", *Wind energy*, 2009; 12: 91-98.

[19] Hansen M.O.L., Johansen J. "Tip studies using CFD with tip loss models", *Wind Energy*, 2004; 7: 343-356.

[20] Yang H., Shen. W.S., Sørensen J., Zhu W.J., "Extraction of airfoil data using PIV and pressure measurements", *Wind Energy*, 2011; 14: 539-556.

[21] Azuma A., Kawachi K., "Local momentum theory and its application to the rotary wing", *Journal of Aircraft*, 1979; 16: 6-14.

[22] Snel H., "Review of Aerodynamics for wind turbines", *Wind Energy*, 2003; 6: 203-211.